IEEE Access
Multidisciplinary | Rapid Review | Open Access Journal

Received March 16, 2021, accepted March 30, 2021, date of publication April 9, 2021, date of current version May 4, 2021.

Digital Object Identifier 10.1109/ACCESS.2021.3072128

Inverse Design for Low Warpage Ultra-Thin Packages Using Constrained Particle Swarm Optimization

CHERYL SELVANAYAGAM[1,2], PHAM LUU TRUNG DUONG[1], BRETT WILKERSON[3], AND NAGARAJAN RAGHAVAN[1], (Member, IEEE)

[1]Engineering Product Development Pillar, Singapore University of Technology and Design, Singapore 487372
[2]Package Engineering, Advanced Micro Devices (AMD) Inc., Singapore 469032
[3]Package Engineering, Advanced Micro Devices (AMD) Inc., Austin, TX 78735, USA

Corresponding author: Cheryl Selvanayagam (cheryl_selavanayagam@mymail.sutd.edu.sg)

This work was supported by the Economic Development Board of Singapore (EDB) and Advanced Micro Devices (AMD) Inc., through the Industry Postgraduate Program (IPP) under Grant IGIPAMD1801.

ABSTRACT Warpage of electronic packages is the result of mismatch in the coefficient of thermal expansion (CTE) between the silicon die (CTE = 2.6ppm/°C) and the substrate (CTE = 15-25 ppm/°C). In ultra-thin packages, the reduced thicknesses can result in even higher package warpage due to the reduced flexural rigidity. Current approaches to minimize warpage include selecting constituent materials in the substrate with lower CTE as well as carrying out copper balancing of metal layers which are equidistant but on opposite sides of the core. In this work, we aim to optimize the metal density of the substrate layers by using an inverse design framework using Particle Swarm Optimization (PSO) with carefully selected constraints to minimize the rework required on the electrical tracing artwork. Results show that the inverse design framework is able to arrive at a 20% reduced warpage by changing local metal densities by just up to 5%. This is a significant reduction in warpage that is achievable by incorporating minor changes to the electrical artwork of the substrate. In future, this methodology can be applied to not only minimize warpage on ultra-thin packages but also enable even thinner ultra-thin package designs to be realized.

INDEX TERMS Bayes method, finite element analysis, global optimization, Markov Chain Monte Carlo (MCMC), material characterization, particle swarm optimization (PSO), substrate, warpage.

I. INTRODUCTION

As packages and silicon dies grow to allow for greater functionality and performance while decreasing in thickness to accommodate the dimensions of the final product they go into, we are fast approaching the limits of the design rules. In order to break free from these constraints, new design methodologies are presently required. Concepts such as inverse design and optimization are key to unlocking better electronic designs in the near future, especially for AI-enabled edge computing applications as well as for 3D integrated circuits requiring heterogeneous integration.

In this work, we have built an inverse design framework which combines data-driven approaches such as Markov Chain Monte Carlo (MCMC), neural networks and global optimization algorithms with physics-based approaches such as finite element analysis and measurements from Digital Image Correlation (DIC) to realize a more optimum design in terms of the overall warpage of the package. Once this framework is established, we use the existing and target warpage profiles and current metal densities as inputs to the optimization routine to determine the locations on the substrate where the metal density should change and by how much in order to approach the target warpage profile. Three case studies with the optimization were carried out with different constraints such that the objective of reducing the current warpage profile by 20% can be achieved, in a manner that can be easily translated to the electrical design of the substrate. In the first case study, the optimization had no constraints. In the second one, the change in metal density at every location was constrained to change within ±5% of the original design and in the third one, a decrease in metal density of up to 30% was used to constrain the optimization.

This study is organized as follows. In Section II, we describe and summarize the warpage-associated

The associate editor coordinating the review of this manuscript and approving it for publication was Kuo-Ning Chiang.

challenges that plague all ultra-thin packages. Section III describes the overall model framework along with each of the three phases that ultimately makes up the inverse design framework. In Section IV, we discuss the results obtained from the optimization and run three case studies to determine how the metal design of the substrate should be tweaked for a lower package warpage. Finally, in Section V, we conclude our study along with some discussions on the scope for future work.

II. THE WARPAGE PROBLEM

Warpage of packages is the result of the large coefficient of thermal expansion (CTE) mismatch between the silicon die (CTE = 2.6ppm/°C) and the organic substrate (CTE = 15-25 ppm/°C). In thin packages, the warpage problem is further exacerbated by the reduced thickness. This phenomenon can be explained by the mechanics of simple plate warpage where flexural rigidity is inversely proportional to the cube of the sample / layer thickness.

The conventional approach to tackling this warpage problem is two-pronged. First, the constituent materials of the substrate are carefully selected for low CTE. Substrate suppliers are continually developing new low CTE materials for the core and Ajinomoto Build-up Film (ABF). Second, copper balancing is carried out on the design where the difference in percentage of copper a certain distance away from both sides of the mid-plane is minimized. However, even perfectly copper balanced printed circuit boards have been found to warp due to different trace directions in the different layers [1]. Once the materials are selected, warpage simulations using finite element analysis (FEA) are carried out to predict the warpage of the part [2]. The accuracy of these simulations, however, are limited by the accuracy of the material properties used for the substrate.

Modelling the electronic substrate can be challenging for several reasons. First, the electronic substrate is a composite material, consisting of alternating layers of metal lines and ABF built up on both sides of the central core. Second, the metal density of the metal layers is non-uniform and with different morphology across the substrate.

This modelling challenge has been addressed to varying degrees of success by two main approaches. The first is a micromechanics approach [3]–[7] that uses the volume fraction of copper in each layer to derive the lumped material properties of the region. When this technique is used, the substrate is assumed to be homogenous with metal density accounted for using the Reuss, Voigt or other formulations [3]–[7]. Valdevit *et al.* have proposed a methodology to account for the different metal features in the various layers of the substrate using this micromechanics approach, with different analytical formulations applied based on the morphology of the copper pattern on the different layers [4].

The second approach is to use trace import simulations where trace geometry is incorporated into the model geometry [5]–[12]. Several authors have demonstrated methodologies which can successfully incorporate the effect of these spatially varying material properties in their simulations, provided the electrical artwork is available to be imported into the simulations [5]–[12]. The volume of work on this topic demonstrates that modelling and optimizing substrate warpage is an important topic in electronic packaging.

In our earlier work, we have shown that accurate inferences about substrate subsection CTEs can be made by incorporating an FEA model with MCMC. The FEA model is used to simulate warpage and this warpage profile is then compared to the experimentally obtained one to determine the error between the two profiles. An MCMC analysis is then used to sample the parameter space to select suitable values for the CTE to be used in the FEA simulations such that error is minimized [13], [14]. This analysis can be made more efficient by using an ANN as a surrogate model for FEA, resulting in analysis time speed up of up to three orders of magnitude with a good accuracy of $R^2 > 0.95$ [15].

We later came up with a surrogate model for warpage based on the underlying metal densities and CTEs and incorporated PSO into this framework so that inverse design can be carried out, where a desired profile is provided to the PSO and the algorithm determines the optimized metal densities that would result in the desired warpage profile [16], [17]. This was demonstrated with 3×3 substrate subsections. A similar framework was also used to learn the stress-strain relationship of materials such as adhesives in the package [18].

In this work, we carry out a global sensitivity analysis to show that in-plane CTE of the substrate has the greatest sensitivity to warpage. We further demonstrate that the proposed framework can be extended to infer the underlying metal densities with the substrate divided into 4×4 substrate subsections. We show comparisons of the PSO performance on 3×3, 4×4 and 5×5 substrate subsections which indicate 4×4 is optimum for low error and fast run time. Finally, we study the effect of adding constraints to the PSO search space so that changes in the metal density can be incorporated in an efficient manner accounting for realistic possible minimal design changes to the trace patterns without perturbing the fundamental design of the stack too much. Without these constraints, the PSO would return solutions that cannot be implemented.

III. OVERALL MODEL FRAMEWORK

The objective of this work is to optimize the metal densities in the substrate of an ultra-thin package such that the warpage of the package may be reduced. Addressing this optimization using conventional approaches such as finite element analysis (FEA) alone or by conducting a series of design of experiments (DOE) would be tedious and expensive. In this work, we propose an AI-assisted modelling framework to achieve this optimization. For computational efficiency, the optimization is run on a surrogate model for warpage which takes into account the metal density at different subsections of the substrate and predicts the resulting warpage profile.

The proposed framework consists of three main phases as shown above in Figure 1. In Phase A, we assemble the

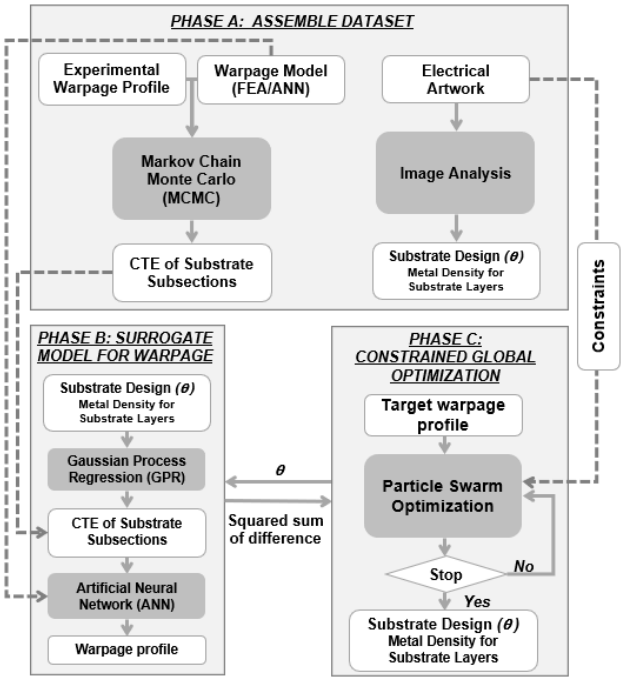

FIGURE 1. **Flow chart showing overall model framework and how the data flows between the different phases. The boxes shaded in grey represent the specific computational tools / methods used in the framework.**

dataset that is required to build a surrogate model for warpage. This dataset consists of the metal density of each layer at each substrate subsection and the corresponding CTE of that subsection. The metal densities are determined by running image analysis on the electrical artwork of each layer of the substrate. The image analysis code works on the basis of counting pixels. The CTE, on the other hand is determined by carrying out a Markov Chain Monte Carlo (MCMC) analysis using the experimental warpage profile from Digital Image Correlation (DIC) and a warpage model from FEA or Artificial Neural Network (ANN).

In Phase B, the datasets assembled in Phase A are used to develop a two-step surrogate model for warpage. We do this using a Gaussian Process Regression (GPR) to tie the substrate metal densities to the CTE and then tie the CTE in turn to the warpage using an ANN. Finally, in Phase C, we used the Particle Swarm Optimization (PSO) routine to determine the optimum metal density in the substrate for the target warpage profile.

A. PHASE A: ASSEMBLING THE DATASET

Before we can create the surrogate model in Phase B, we first need to gather and augment the training dataset for the surrogate model. Specifically, we require the coefficient of thermal expansion (CTE), that has been identified as the material property with the greatest sensitivity to warpage of the part, and its correlation to the corresponding metal layer densities at each substrate subsection.

1) CTE OF SUBSTRATE SUBSECTIONS

The CTE of each substrate subsection was determined using the data-driven approach of Markov Chain Monte Carlo (MCMC) with the physics-driven approach of FEA. The MCMC is a subset of Bayesian inference [19], [20]. Bayesian inference allow us to update our belief about an event (or its probability) based on new data. With MCMC, the Monte Carlo property results in the algorithm randomly sampling the parameter space to determine a new posterior (probability of the event given the data). The Markov Chain property means only the current and new values for posterior are compared to determine whether the new parameter is accepted and added to the chain (sequence) of accepted parameters. Finally, the probability density function of the parameters in the chain determine the most probable value for the parameter capturing the spread / uncertainty in its estimation too. This approach of MCMC driven directly by FEA has been previously described in detail and shown to be effective in predicting the CTE of the substrate subsections accurately [13], [14], though it can be time-consuming. For instance, 1000 iterations of an MCMC analysis driven by FEA simulations to infer four parameters takes about 6 hours to complete. As the number of parameters to infer increases, so does the number of MCMC iterations for successful convergence and hence analysis time.

We have also previously demonstrated that using an ANN as a surrogate model for FEA results in a speed up of up to three orders of magnitude with a very good accuracy of $R^2 > 0.95$ [15]. As opposed to surrogate models such as linear and quadratic approximations and the response surface method, ANNs can accommodate a large number of inputs and outputs without significant impact on error, provided the training dataset is large enough [21], [22]. The MCMC/FEA approach was made more computationally efficient by replacing the FEA model with an ANN that has been trained on the FEA inputs and outputs [16]–[18].

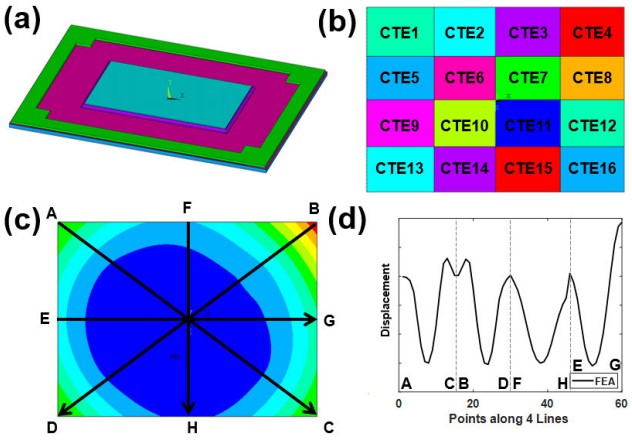

FIGURE 2. **Details of FEA model (a) 3D model (b) substrate divided into 16 subsections with unique CTEs (c) four lines along which the warpage profile is probed (d) sample result of warpage profile along the four lines concatenated together to represent the overall warpage pattern.**

The MCMC/ANN approach is used here. The 3D FEA quarter model consisting of the die, substrate and stiffener, as shown in Fig. 2(a). Substrate area is less than 1600mm^2 with die size less than 200mm^2. Total thickness of the package is less than 1.5mm. In order to represent the varying metal densities across the substrate (which would result in varying CTEs across the substrate), we divide the substrate into different subsections. For example, in Fig. 2(b), we divide the substrate into a 4×4 array. A unique CTE is then assigned to each of the resulting 16 segments. The substrate warpage profile along the four lines (Fig. 2(c)) is then extracted from the results of the FEA simulation and plotted separately as shown in Fig. 2(d). All materials are assumed to be linear elastic with temperature-dependent properties assigned to the first-level interconnect layer. The loading condition was a single step temperature ramp down from 150°C to room temperature.

The training dataset for the ANN is generated by running this FEA simulation for 100 runs, each time with a different set of 16 CTEs as inputs and generating the corresponding warpage profiles. Once trained, the ANN is coupled with the MCMC and the warpage profile from Digital Image Correlation (DIC) to infer the most probable CTE for each segment. The entire MCMC analysis is automated and carried out in Matlab®using the MCMC toolbox developed by Marko Laine [23]. As the number of MCMC iterations is in the order of a few thousands, using the surrogate model instead of FEA will result in a significant speed up of the simulation flow by three orders of magnitude. Our results (in the future sections) show that there is indeed very good correlation in the warpage profile comparing that based on the CTE inferred by the MCMC and the experimental measurements of warpage.

2) METAL DENSITY FOR SUBSTRATE SUBSECTIONS

An image analysis by pixel counting on each layer of the electrical artwork of the substrate was carried out using Matlab ® to determine the metal density. The image of the entire layer is converted to a greyscale image, it is cropped equally according to the number of subsections and then the metal density of each subsection is calculated as the number of grey pixels in the subsection over the total number of pixels in the subsection.

3) AUGMENTING THE DATASET

Running this analysis once with a substrate divided into 4×4 segments would result in a dataset consisting of 16 datapoints. This is far too few datapoints to train the surrogate model. To increase the size of the training dataset, we run this entire analysis 12 times, each time with the substrate divided into a different number of segments. There is a limit to the number of subsections that the MCMC can accurately accommodate. Through experimenting with the code, we have found that 25 CTEs can still be inferred accurately for the analysis we are conducting. With more substrate subsections, a larger number of FEA runs is required to train the ANN. The substrate subsections considered and the corresponding FEA runs to train the ANN are detailed in Table 1. In this manner, the training dataset for the surrogate model was enhanced from a mere 16 all the way up to 232.

TABLE 1. List of substrate subsections used.

Substrate Subsections	No. of Datapoints for Phase B	Training Dataset Size from FEA
2×2	4	100
3×3	9	100
4×4	16	200
5×5	25	200
5×4	20	200
4×5	20	200
3×7	21	200
7×3	21	200
4×6	24	200
6×4	24	200
3×8	24	200
8×3	24	200
Total	232	2200

B. PHASE B: SURROGATE MODEL FOR WARPAGE

In Phase B, we build a surrogate model for warpage using a sequence of GPR and an ANN, which when given the metal density of the substrate subsection across the different layers, calculates the final resulting warpage profiles across the substrate. A similar surrogate model for warpage was used in our previous work for optimization studies with reasonably good results [16], [17]. The key improvement over our previous work is that we have extended this model to 4×4 subsections, instead of 3×3 used previously to enhance the spatial resolution of the analysis.

1) GAUSSIAN PROCESS REGRESSION (GPR)

The Gaussian Process Regression (GPR) was selected as the surrogate model to link the metal densities on the eight layers of the substrate to the CTE. We selected the GPR over the ANN here based on the prediction error as the error metric was significantly larger for the ANN. As the sample size is still relatively small, a k-fold cross-validation training methodology was adopted with $k = 10$. In our previous work, a k-value larger than 10 was used, resulting in the GPR model overfitting the training dataset. While this resulted in low errors for the training dataset, the errors were large for the test dataset though. With a k-value of 10, there are several points that are not predicted accurately but the overall GPR performance is still significantly better than the ANN as shown in Figure 3. We used an eight-parameter vector describing the metal density on each of the eight layers of the substrate and the corresponding CTE, both of which were determined in Phase A.

2) ARTIFICIAL NEURAL NETWORK (ANN)

For the prediction of the warpage profile given the CTE, we used an ANN as the surrogate model because this has already been established in Phase A and has good accuracy.

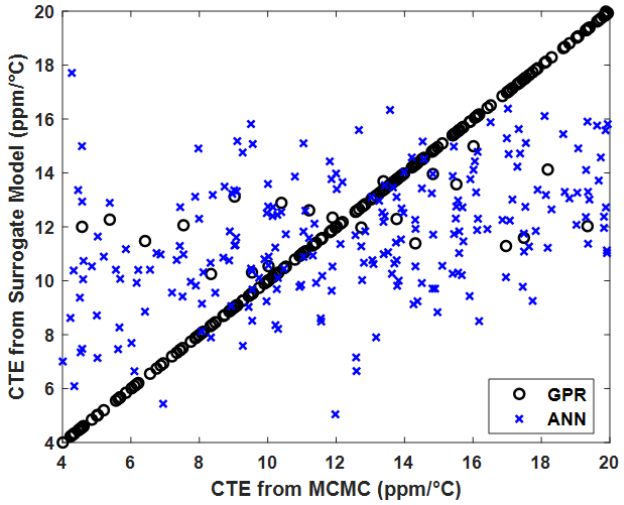

FIGURE 3. Scatter plot showing CTE obtained from MCMC and that from GPR and ANN surrogate models. CTE from GPR correlates to MCMC output significantly better than the ANN.

These two models combined together represent the overall surrogate model for warpage. The GPR converts the input vector of 128 elements ($4 \times 4 \times 8$ layers $= 128$) into a CTE vector of 16 elements ($4 \times 4 = 16$ substrate subsections). The ANN then uses the 16-element CTE vector to compute the warpage profile along the 4 lines.

C. PHASE C: CONSTRAINED GLOBAL OPTIMIZATION

Finally, in Phase C, we optimize the metal density by running the global optimization algorithm (Particle Swarm Optimization) on the surrogate model for warpage from Phase B. As we provide the target warpage profile to the algorithm for the optimization, this approach can also be thought of as enabling inverse design of the substrate. The inverse design approach starts with the desired outcome and through the use of AI and optimization algorithms, the material properties or design parameters that enable us to approach the desired outcomes as closely as possible are determined. Similarly here, we specify the final desired target warpage profile and the output from the algorithm are the metal density over the substrate that will result in that warpage. Again, for this analysis, Matlab® and the Global Optimization toolbox in it was used [24].

IV. RESULTS AND DISCUSSION

A. GLOBAL SENSITIVITY STUDY

We first carried out a global sensitivity analysis to determine which materials and material properties in the substrate have the largest contribution to the warpage of the part. We focused on the substrate and stiffener adhesive as these materials are easily tunable for reduced warpage whereas die and stiffener materials are fixed. The material properties considered for the substrate include the Young's Modulus (E), in plane and out of plane CTE (CTE_{x-y}, CTE_z), yield stress (σ_y) and tangent modulus (E_t). For the adhesive, as it is an isotropic material, the same material properties were considered but with a single value for CTE.

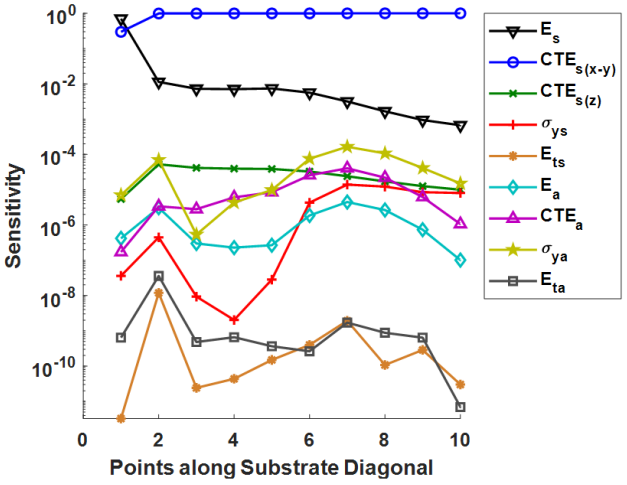

FIGURE 4. Plot showing results of sensitivity analysis to study which parameters have the largest impact on substrate warpage plotted on logarithmic scale. In-plane CTE (CTE_{x-y}) has the greatest sensitivity.

The first order sensitivity coefficients indicate the contribution of each individual parameter towards the total model variance. This is shown in Figure 4 on a logarithmic scale in order to be able to visualize the significantly smaller contributions of some of the parameters. In-plane CTE dominates warpage behavior. This is followed by the substrate modulus, with a first order sensitivity coefficient which is two orders of magnitude lower. As the in-plane CTE is the most sensitive parameter, that is the only parameter considered in this framework.

B. MARKOV CHAIN MONTE CARLO (MCMC)

The MCMC analysis was carried out 12 times with the substrate divided into different subsections as shown in Table 1. The CTEs obtained from this analysis are shown graphically in Figure 5. This figure shows how the size and shape of each substrate subsection changes when divided differently. The difference in size and shape adds depth to the dataset for training the surrogate model in Phase B as the metal layer density and morphology in these regions would be significantly different. We observe from Figure 5 that a larger number of subsections result in a finer resolution CTE output. The CTE between adjacent substrate subsections can be quite different and this is attributed to the wide variations in underlying metal densities.

Figure 6 shows the displacement plots obtained from the ANN (surrogate model for CTE to warpage) using the CTEs inferred by the MCMC for each of the 12 substrate subsection patterns. Though there is larger error at the start and the end points of the four lines, in general the inferred CTEs result in displacement plots that look very similar to that obtained experimentally. This indicates that the MCMC is providing reasonable inference of CTE in all cases even when trying to fit a larger number of variables.

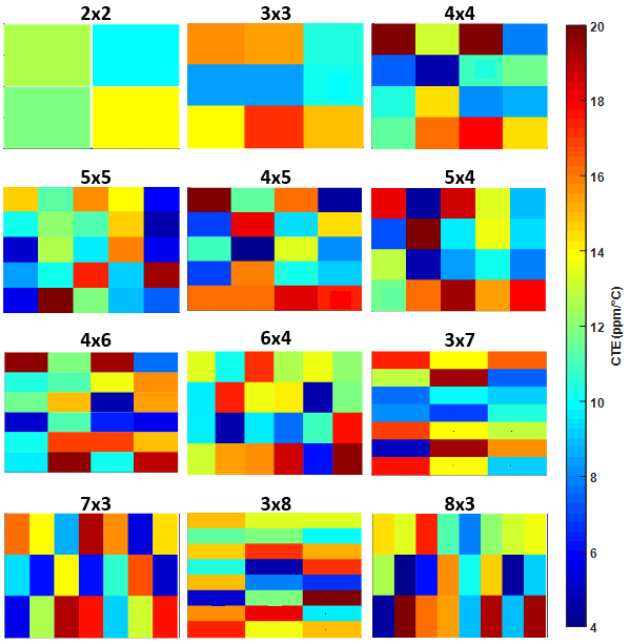

FIGURE 5. Graphical representation of CTE inferred from MCMC analysis with the substrate divided into different subsections. Depending on the underlying metal densities, even adjacent substrate subsections can exhibit very different CTEs. Different subsections were used to augment the training dataset used to train the surrogate model in Phase B.

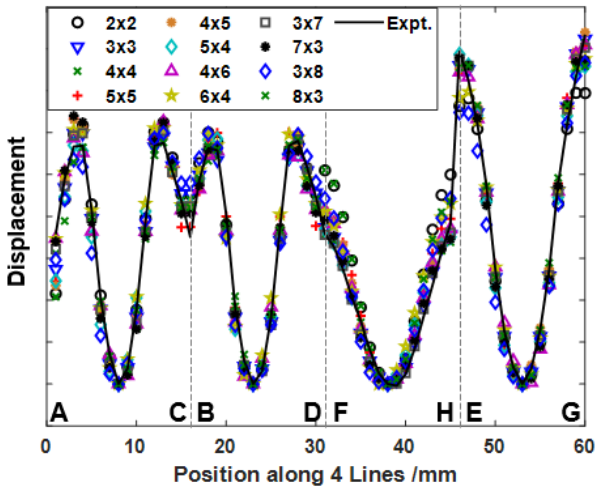

FIGURE 6. Displacement plots obtained from ANN using CTE values from MCMC. In general, the displacement plot correlate well to the experimental one, indicating that the CTEs from MCMC are accurate.

C. PARTICLE SWARM OPTIMIZATION (PSO)

Particle swarm optimization [25] was first introduced in 1995 with applications to optimizing continuous non-linear functions and training neural networks. Since then, the optimization algorithm has gained popularity due to its ability to converge faster compared to genetic algorithms. Here, the objective is to determine the optimize metal density such that the error between the warpage profile from measurements and that from the surrogate model is minimized. In each instance the swarm size was varied from 100 to 200 particles to determine the optimum swarm size for reduced error. Default values for self-adjustment weight and social-adjustment weight of 1.49 were accepted in all cases. The analysis terminates when the relative change in the objective value over the last 20 iterations is less than 1×10^{-6}.

The PSO was first carried out using the baseline experimental warpage profile to check whether similar CTEs and metal densities to the substrate used in the experiments would be obtained. This analysis was carried out using the substrate with subsections 3×3, 4×4 and 5×5. Larger number of substrate subsections would increase the resolution of the metal density optimization at the expense of analysis time. Subsequently, this framework was used to study what changes to the metal densities are required for a 20% reduced warpage profile. We also considered three case studies here where constraints were introduced to the PSO search space such that recommended changes to the metal density would be easier and more practical to implement from an electrical-mechanical co-design point of view. These include limiting the percentage change in metal density to within $\pm 5\%$ at each substrate subsection and implementing a "decrease only" rule to the PSO as it is easier to remove metal from the design than to add to it.

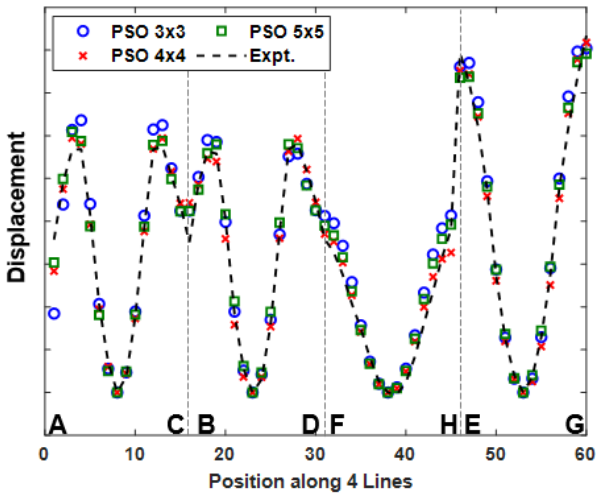

FIGURE 7. Displacement plots obtained from PSO for models using substrate subsections 3×3, 4×4 and 5×5 compared to the experimental profile. The model with 3×3 subsections has a higher deviation than the other two models.

1) PSO USING BASELINE WARPAGE PROFILE FROM EXPERIMENTS

Results from the PSO analysis which were carried out using the substrate with subsections 3×3, 4×4 and 5×5 are shown in Figures 7 to 10. Figure 7 shows the final displacement profile obtained from the PSO for the analysis using substrate subsections 3×3, 4×4 and 5×5 compared to the original warpage profile from experiment that we are trying to replicate. There is a slightly higher deviation observed with 3×3 substrate subsections compared to 4×4 and 5×5. This deviation is quantified in terms of the sum squared error between the PSO output and the experimental warpage profile

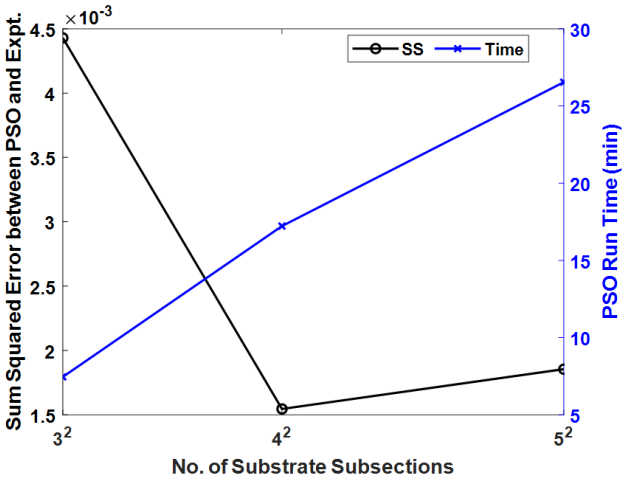

FIGURE 8. Plot of sum square errors and PSO run time for models with substrate subsections 3 × 3, 4 × 4 and 5 × 5 compared to the experimental profile. Lowest sum squared error is with 4 × 4 substrate subsections.

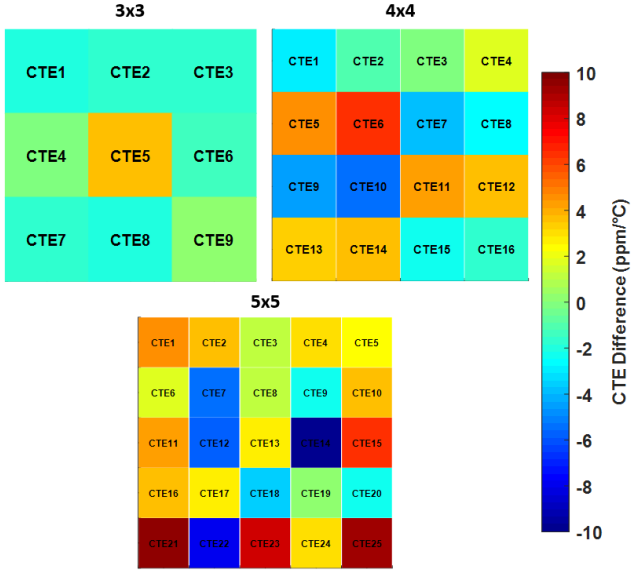

FIGURE 9. Graphical representation of the difference between the intermediate CTE from PSO and that inferred by MCMC. As the number of substrate subsections increase, so does the maximum CTE difference.

on Figure 8. Also plotted on Figure 8 is the time taken for the PSO analysis. The analysis with 4 × 4 subsections is the middle ground for low sum squared error and reasonable simulation time. The reduced SS from the cases with 4 × 4 and 5 × 5 substrate subsections shows that the greater spatial resolution improves the accuracy of the analysis. There is a slight increase in SS with 5 × 5 substrate subsections as the PSO has a much larger number of variables to optimize.

The difference between the intermediate CTE values obtained from the PSO and that inferred from the MCMC is shown in Figure 9. As the number of subsections increase, the deviation in CTE between the PSO and MCMC also increases. The maximum CTE difference in a 3 × 3 substrate subsection is 2.9 ppm/°C. This increases to 7.3 and 9.7ppm/°C with 4 × 4 and 5 × 5 substrate

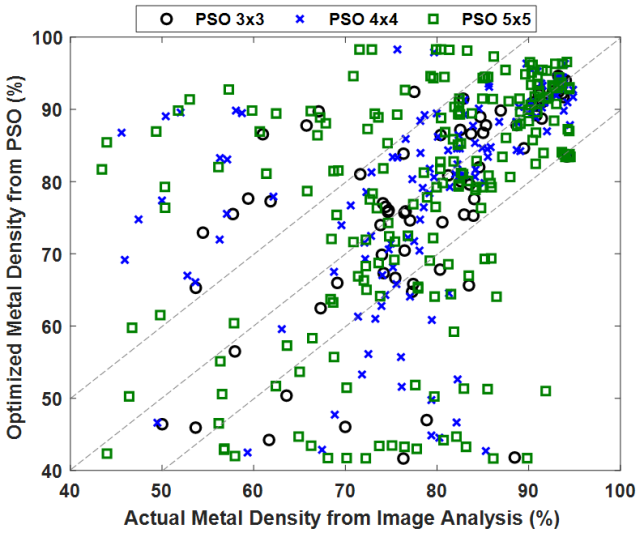

FIGURE 10. Scatter plot of the metal density of each substrate subsection obtained from image analysis and PSO. Larger scatter outside the ±10% error bands is observed as the number of substrate subsections increases. The proportion of datapoints falling outside the ±10% range with 3 × 3, 4 × 4 and 5 × 5 substrate subsections is 28%, 31% and 40% respectively.

subsections respectively. A similar trend is observed in Figure 10 where we plot the metal density obtained from image analysis against that obtained from PSO. With more substrate subsections, there are a larger proportion of points falling outside the ±10% range. With 3 × 3, 4 × 4 and 5 × 5 substrate subsections, the proportion of datapoints falling outside the ±10% range is 28%, 31% and 40% respectively. In making these comparisons, we are assuming that there is only one unique solution to the metal density and CTE which results in the experimental warpage profile which is probably not true. Still, we can confidently claim that the increased errors with 5 × 5 points is due to the increased complexity associated with more variables. In order to reconcile the reduced spatial resolution with a fewer substrate subsections, and the larger error associated with optimizing over larger search spaces with a larger number of substrate subsections, the rest of the optimizations carried out in this section will focus on substrate subsections of 4 × 4.

2) CASE STUDY 1: DESIGNING FOR 20% REDUCED WARPAGE WITHOUT CONSTRAINTS

In this section, we used the framework to determine the metal density map that would result in a reduction of warpage by 20% without imposing any constraints at all. To test out the effectiveness and validity and limits of the optimization framework, we started with an experimental warpage profile that has been reduced by 20% and used the PSO to search for the appropriate metal density map that would result in this warpage. The change in CTE and metal density maps are shown in Figures 11 and 12. In this initial model, the PSO search space was purposely left unconstrained. Analysis reveals that the resulting CTE map requires changes at some subsections by up to 8 ppm/°C. The resulting metal density

map calls for large changes in metal density from a decrease of 40% to an increase of 45% at certain locations of certain layers of the substrate which is not feasible to implement without disrupting the basic electrical design artwork.

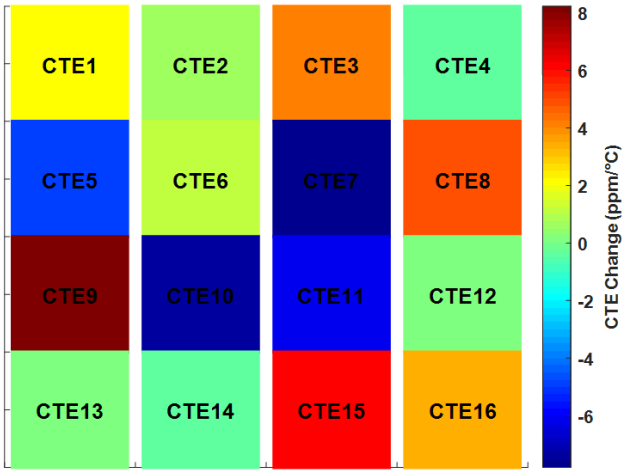

FIGURE 11. Graphical representation of the CTE change recommended by PSO for a 20% reduced warpage compared to the experimentally obtained one.

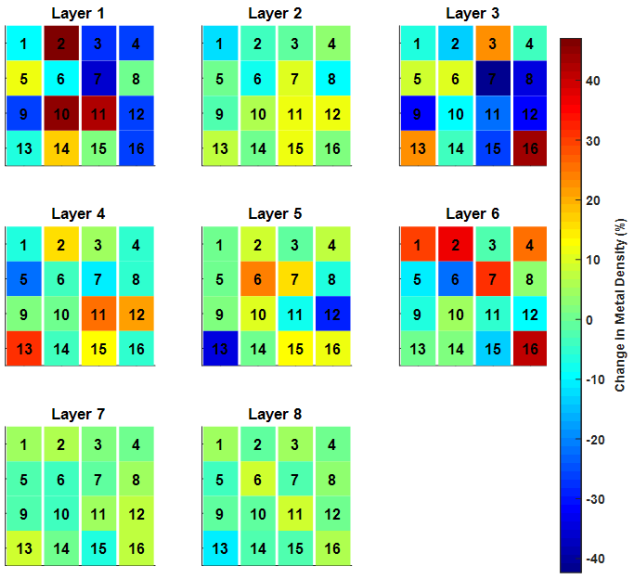

FIGURE 12. Graphical representation of the metal density changes needed based on inferences from PSO using the original warpage profile and PSO considering the 20% reduced warpage with no other imposed constraints.

3) CASE STUDY 2: DESIGNING FOR 20% REDUCED WARPAGE WITH METAL DENSITY CHANGE CONSTRAINED TO WITHIN ±5%

Next, we implemented a constrained PSO where the upper and lower bounds of the search space is constrained to within ±5% of the original metal density. Again, the CTE and metal density change maps are shown in Figures 13 and 14. As a result of the applied constraints, the change in CTE and metal density required to achieve the 20% reduction in warpage is

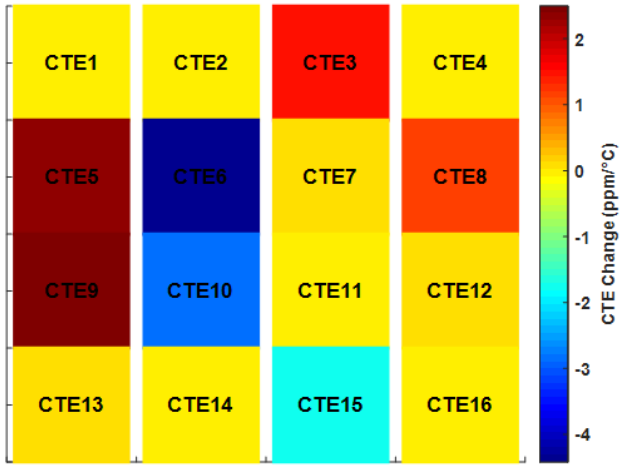

FIGURE 13. Graphical representation of CTE change between PSO using the original warpage profile and the PSO using the 20% reduced one with metal density changes constrained to ±5%.

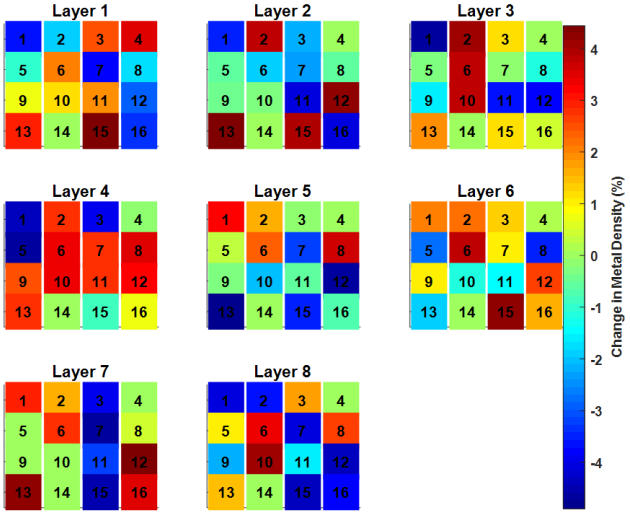

FIGURE 14. Graphical representation of metal density change between PSO using the original warpage profile and the PSO considering 20% reduced warpage with metal density changes constrained to ±5%.

significantly reduced. The maximum change in CTE required is about 4 ppm/°C and the maximum change in metal density requires at any location is 5%, as required by the applied constraint. While in Figure 12, some layers in the substrate (Layer 2, 7 and 8) are exempted from large changes in metal density; in Figure 14, all the layers and subsections undergo a seemingly random distribution of increases and decreases in metal density, indicating that the optimization is severely constrained. Naturally, these additional constraints applied to the search space result in a displacement profile that deviates from the design profile.

As shown in Figure 15, while a PSO with no constraints can arrive at the design profile quite accurately (SS $= 2.3 \times 10^{-3}$), the PSO with constraints deviates at certain sections, resulting in an SS of 6.9×10^{-3}. These metal density changes with the constraints will still be useful as the final warpage of the part is determined as the difference

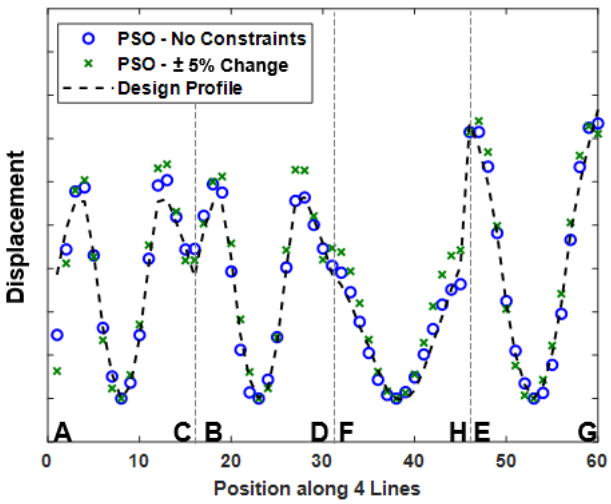

FIGURE 15. Displacement plots obtained from PSO with no constraints and with metal density change constrained to ±5% compared to the design profile.

between the maximum and minimum of the displacement profile. For the PSO with constraints, this warpage quantity still meets the requirement of a 20% reduction, even if the displacement profile does not exactly match the 20% reduced profile. More importantly, these changes will be easier to incorporate into the metal density design with minimal disruption to electrical performance.

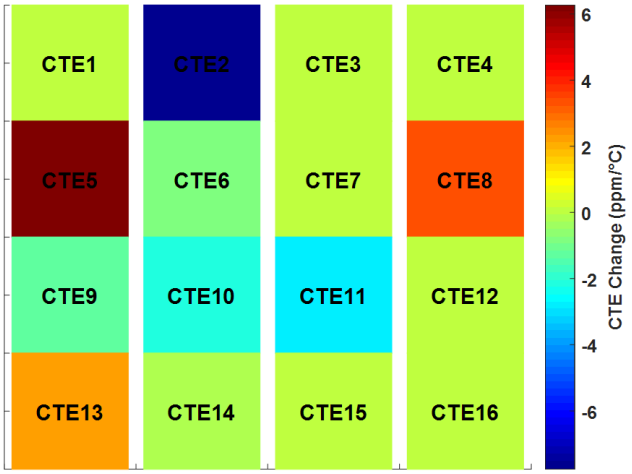

FIGURE 16. Graphical representation of CTE change between PSO using the original warpage profile and the PSO using the 20% reduced one with metal density changes constrained to decrease by up to 30%.

4) CASE STUDY 3: DESIGNING FOR 20% REDUCED WARPAGE WITH METAL DENSITY CHANGE CONSTRAINED TO DECREASE BY 30%

Tweaking substrate design is easier to accomplish if the local metal density is decreased as this can be accomplished by removing metal by simply adding features like degassing holes. Increasing the metal density might not always be easily accomplished as adding these features can interfere with the electrical design and associated cross talk compromising on

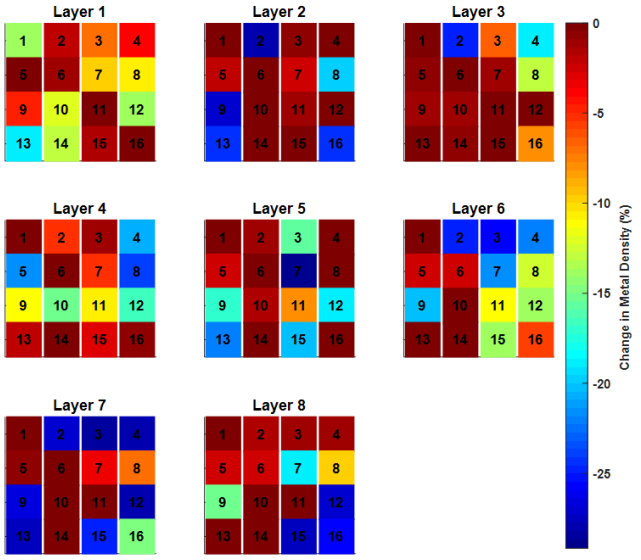

FIGURE 17. Graphical representation of metal density change between PSO using the original warpage profile and the PSO using the 20% reduced one with metal density changes constrained to decrease by up to 30%.

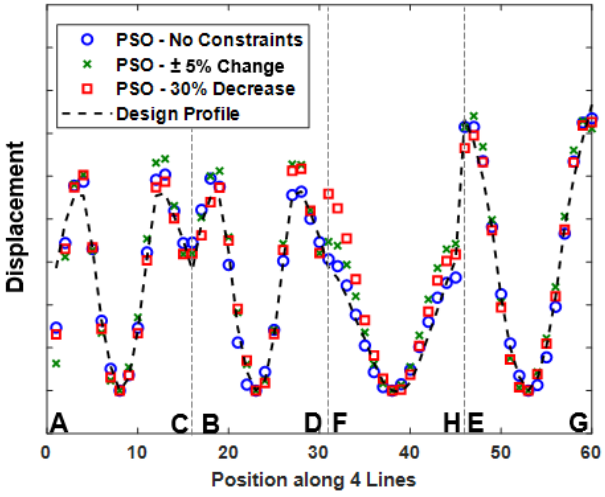

FIGURE 18. Displacement plots obtained from PSO with no constraints applied and with two different constraints applied to the metal density change (±5% and decrease up to 30%) compared to the design profile. Note that the zero displacement reference point corresponds to the center of the substrate.

the electrical signal integrity and reliability. In this section, we run the optimization with the constraint that the metal density at each region can only decrease by up to 30%.

The corresponding results are shown in Figures 16 to 18. Figures 16 and 17 show the CTE and metal density maps respectively. The maximum CTE change is about 6 ppm/°C and the maximum decrease in metal density required is about 30%. Figure 17 shows that the optimization is severely limited by the 'decrease only' constraint as many locations on the substrate subsections are at zero change in metal density. Figure 18 shows the displacement plot for all three case studies on one plot - with no constraints applied, with a constraint of metal density change of ±5% and with a constraint of

TABLE 2. Summary of case study results.

Case Study	PSO Constraint	Min. and Max. CTE Change between PSO and desired warpage profile (min/max) (ppm/^{0}C)	SS between PSO and desired warpage profile
1	No constraint	-7.8 / 8.2	2.3×10^{-3}
2	Metal density change constrained to within ±5%	-4.4 / 2.5	6.9×10^{-3}
3	Metal density change constrained to decrease by up to 30%	-7.8 / 6.7	6.3×10^{-3}

metal density decrease of up to 30%. Table 2 summarizes the minimum and maximum CTE change as well as the SS between the PSO and the desired warpage profile. Akin to the observed trends in the previous section with the imposed constraint of ±5% change, the PSO with up to 30% decrease also results in a higher SS of 6.3×10^{-3} between the PSO and the desired warpage profile. It is also interesting to note that large local changes in CTE (as observed in Case Studies 1 and 3) do not necessarily result in a lower SS, indicating that CTEs of all locations contribute to the warpage profile and not only the subsections where large changes occur.

V. CONCLUSION AND RECOMMENDATIONS

In this work, we have developed an inverse design framework to design low warpage substrates by making changes to the underlying metal density distribution across the multiple layers of the substrate. We do this by using physics-driven approaches like FEA and data-driven approaches like MCMC and global optimization with carefully selected constraints. Results from implementing this framework indicate that a significant reduction in warpage of an ultra-thin package of 20% can be achieved through various tweaks to the local metal densities. We have demonstrated that a wide range of constraints such as a mere ±5% change or up to a 30% decrease in local metal densities can easily and effectively enable this reduction in warpage. These changes in the substrate metal design are small enough to be incorporated during the substrate design stage, without requiring a complete redesign of the substrate. We could not have arrived at this outcome using FEA simulations alone due to the sheer volume of simulations and analysis time that would have been required.

One drawback of this approach using MCMC is that the solution is not unique and there could be many substrate subsection CTE combinations that result in the same warpage profile. In future, this drawback will be addressed by including an additional module into the framework to determine the substrate subsection CTE using FEA instead of MCMC. We will also continue to further verify these results using trace import simulations and build samples to measure the actual warpage improvements. The framework presented in this paper is modular and can be paired with any suitable surrogate model or optimization algorithm. The choice of surrogate model and optimization algorithm is problem-specific, with different models and algorithms working more accurately and efficiently for different datasets. Other options for the surrogate model include random forest and support vector machine. While we have focused on PSO here, we also plan to explore other optimization algorithms such as cross entropy and genetic algorithm to evaluate how they perform in comparison to the PSO that is used here. Finally, we will implement tensor train decomposition to analyze the warpage patterns across the entire surface of the substrate instead of just along the four diagonal lines. In other words, we will aim to solve the inverse design problem in two dimensions rather than just one.

ACKNOWLEDGMENT

AMD, the AMD Arrow logo, and combinations thereof are trademarks of Advanced Micro Devices, Inc. Other product names used in this publication are for identification purposes only and may be trademarks of their respective companies.

REFERENCES

[1] P. Hutapea and J. L. Grenestedt, "Tuning of electric artworks of printed circuit boards to reduce warpage," in *Proc. 9th Int. Symp. Adv. Packag. Mater., Processes, Properties Interfaces*, Atlanta, GA, USA, 2004, pp. 230–234.

[2] Y. Kim, A.-Y. Park, C.-L. Kao, M. Su, B. Black, and S. Park, "Prediction of deformation during manufacturing processes of silicon interposer package with TSVs," *Microelectron. Rel.*, vol. 65, pp. 234–242, Oct. 2016.

[3] C. Selvanayagam, R. Mandal, and N. Raghavan, "Comparison of experimental, analytical and simulation methods to estimate substrate material properties for warpage reliability analysis," *Microelectron. Rel.*, vols. 88–90, pp. 817–823, Sep. 2018.

[4] L. Valdevit, V. Khanna, A. Sharma, S. Sri-Jayantha, D. Questad, and K. Sikka, "Organic substrates for flip-chip design: A thermo-mechanical model that accounts for heterogeneity and anisotropy," *Microelectron. Rel.*, vol. 48, no. 2, pp. 245–260, 2008.

[5] S. Shantaram and T. Hauck, "Methodology for predicting BGA warpage by incorporating metal layer design," in *Proc. Int. Symp. Microelectron. (IMAPS)*, San Diego, CA, USA, 2014, pp. 37–43.

[6] V.-L. Pham, H. Wang, J. Xu, J. Wang, S. Park, and C. Singh, "A study of substrate models and its effect on package warpage prediction," in *Proc. IEEE 69th Electron. Compon. Technol. Conf. (ECTC)*, Las Vegas, NV, USA, May 2019, pp. 1130–1139.

[7] L. O. McCaslin, S. Yoon, H. Kim, and S. K. Sitaraman, "Sitaraman, Methodology for modeling substrate warpage using copper trace pattern implementation," *IEEE Trans. Adv. Packag.*, vol. 32, no. 4, pp. 740–745, Nov. 2009.

[8] M. Wang and B. Wells, "Substrate trace modeling for package warpage simulation," in *Proc. IEEE 66th Electron. Compon. Technol. Conf. (ECTC)*, Las Vegas, NV, USA, May 2016, pp. 516–523.

[9] V. K. Yaddanapudi, S. Krishnaswamy, R. Rath, and R. Gandhi, "Validation of new approach of modelling traces by mapping mechanical properties for a printed circuit board mechanical analysis," in *Proc. IEEE 17th Electron. Packag. Technol. Conf. (EPTC)*, Singapore, Dec. 2015, pp. 1–6.

[10] P. Chen, Z. Ji, Y. Liu, C. Wu, N. Ye, and H. Takiar, "Warpage prediction methodology of extremely thin package," in *Proc. IEEE 67th Electron. Compon. Technol. Conf. (ECTC)*, Orlando, FL, USA, May 2017, pp. 2080–2085.

[11] S. P. Gurrum, G. Li, H.-Y. Lin, and Y. Lin, "An image-based effective property method for strip warpage modeling," in *Proc. IEEE 66th Electron. Compon. Technol. Conf. (ECTC)*, Las Vegas, NV, USA, May 2016, pp. 2034–2039.

[12] B. Kim and B. Han, "Numerical/experimental hybrid approach to predict warpage of thin advanced substrates," in *Proc. IEEE 68th Electron. Compon. Technol. Conf. (ECTC)*, San Diego, CA, USA, May 2018, pp. 267–272.
[13] C. Selvanayagam, P. L. T. Duong, R. Mandal, and N. Raghavan, "Machine learning approach to improve accuracy of warpage simulations," in *Proc. IEEE 69th Electron. Compon. Technol. Conf. (ECTC)*, Las Vegas, NV, USA, May 2019, pp. 834–841.
[14] C. Selvanayagam, P. L. T. Duong, and N. Raghavan, "Learning localized spatial material properties of substrates in ultra-thin packages using Markov chain Monte Carlo and finite element analysis," *IEEE Access*, vol. 8, pp. 50163–50170, 2020.
[15] C. Selvanayagam, R. Mandal, P. L. T. Duong, and N. Raghavan, "Neural network assisted speed up of high fidelity warpage simulations towards design for reliability in ultra-thin packages," in *Proc. IEEE CPMT Symp. Jpn. (ICSJ)*, Kyoto, Japan, Nov. 2019, pp. 89–93.
[16] C. Selvanayagam, P. L. T. Duong, and N. Raghavan, "AI-assisted package design for improved warpage control of ultra-thin packages," in *Proc. 21st Int. Conf. Thermal, Mech. Multi-Phys. Simulation Exp. Microelectron. Microsyst. (EuroSimE)*, Cracow, Poland, Jul. 2020, pp. 1–7.
[17] C. Selvanayagam, P. L. T. Duong, and N. Raghavan, "Inverse design of substrate from warpage surrogate model using global optimisation algorithms in ultra-thin packages," in *Proc. IEEE 70th Electron. Compon. Technol. Conf. (ECTC)*, Orlando, FL, USA, Jun. 2020, pp. 2309–2316.
[18] C. Selvanayagam, P. L. T. Duong, and N. Raghavan, "Learning the stress-strain relationships of ultra-thin package materials using a Bayesian approach," in *Proc. IEEE 70th Electron. Compon. Technol. Conf. (ECTC)*, Lake Buena Vista, FL, USA, Jun. 2020, pp. 1638–1645.
[19] D. Gamerman and H. Lopes, *Markov Chain Monte Carlo*. New York, NY, USA: Chapman & Hall, 2006.
[20] D. P. Kroese, T. Taimre, and Z. I. Botev, *Handbook of Monte Carlo Methods* (Wiley Series in Probability and Statistics). New York, NY, USA: Wiley, 2011.
[21] R. Rojas, *Neural Networks: A Systematic Introduction*. Berlin, Germany: Springer-Verlag, 1996.
[22] C. F. Higham and D. J. Higham, "Deep learning: An introduction for applied mathematicians," 2018, *arXiv:1801.05894*. [Online]. Available: http://arxiv.org/abs/1801.05894
[23] H. Haario, M. Laine, A. Mira, and E. Saksman, "DRAM: Efficient adaptive MCMC," *Statist. Comput.*, vol. 16, pp. 339–354, Dec. 2006, doi: 10.1007/s11222-006-9438-0.
[24] *MATLAB 2019a Global Optimization Toolbox User Guide*, MathWorks, Natick, MA, USA, 2019.
[25] J. Kennedy and R. Eberhart, "Particle swarm optimization," in *Proc. Int. Conf. Neural Netw. (ICNN)*, Perth, WA, Australia, vol. 4, 1995, pp. 1942–1948.

CHERYL SELVANAYAGAM received the bachelor's and master's degrees in mechanical engineering from the National University of Singapore (NUS). She is currently pursuing the Ph.D. degree with the Singapore University of Technology and Design (SUTD). She is also a member of Technical Staff with Advanced Micro Devices (AMD), Singapore. She has worked on material characterization and mechanical simulations at the A∗STAR Institute of Microelectronics (IME), Singapore. Her current research interest includes incorporation of machine learning algorithms with high-fidelity finite element simulations for warpage minimization in ultra-thin electronic packages.

PHAM LUU TRUNG DUONG received the B.S. and M.S. degrees in electrical engineering from Bauman Moscow State Technical University, in 2006 and 2008, respectively, and the Ph.D. degree in process control from Yeungnam University, South Korea, in 2013. He is currently a Senior Research Scientist with the Engineering Product Development (EPD) Pillar, Singapore University of Technology and Design (SUTD). His research interests include PID control, model predictive control, stochastic systems, prognostics and health management, and uncertainty quantification.

BRETT WILKERSON has been a Principal Member of Technical Staff (Product Development Engineer) with Advanced Micro Devices (AMD), Austin, TX, USA, since 2015. He currently works on the development of advanced packaging technology with focus on heterogeneous integration (2.5D, 3D, and WLFO) and manages alignment of new foundry technology to packaging (CPI, PDKs, and Technology Qualification). Prior to this, he spent 15 years as a Semiconductor Packaging Engineer with Freescale Semiconductors, TX, USA.

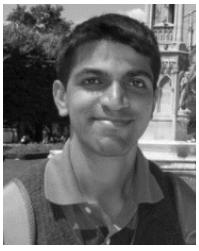

NAGARAJAN RAGHAVAN (Member, IEEE) received the Ph.D. degree in microelectronics from the Division of Microelectronics, Nanyang Technological University (NTU), Singapore, in 2012. He is currently an Assistant Professor with the Engineering Product Development (EPD) Pillar, Singapore University of Technology and Design (SUTD). Prior to this, he was a Postdoctoral Fellow with the Massachusetts Institute of Technology (MIT), Boston, and IMEC, Belgium, in joint association with the Katholieke Universiteit Leuven (KUL). He has authored/coauthored more than 200 international peer-reviewed publications and five invited book chapters as well. His work focuses on reliability assessment, characterization, and lifetime prediction of nanoelectronic devices as well as material design for reliability, inverse design, physics informed machine learning, uncertainty quantification, and prognostics and health management of electronic systems. He was an Invited Member of the IEEE GOLD Committee from 2012 to 2014. He was a recipient of the IEEE Electron Device Society (EDS) Early Career Award for 2016, an Asia-Pacific recipient of the IEEE EDS Ph.D. Student Fellowship in 2011 and the IEEE Reliability Society Graduate Scholarship Award in 2008. He serves as the General Chair for IEEE IPFA 2021 at Singapore and has consistently served on the review committee for various IEEE journals and conferences, including IRPS, IIRW, IPFA, and ESREF. He is currently serving as an Associate Editor for IEEE Access.